Chinese Journal of Catalysis 43 (2022) 1842–1850

available at www.sciencedirect.com

ScienceDirect

journal homepage: www.sciencedirect.com/journal/chinese-journal-of-catalysis

Article

Ultrathin 3D radial tandem-junction photocathode with a high onset potential of 1.15 V for solar hydrogen production

Shaobo Zhang [a], Huiting Huang [b], Zhijie Zhang [a], Jianyong Feng [b], Zongguang Liu [a], Junzhuan Wang [a], Jun Xu [a], Zhaosheng Li [b,*], Linwei Yu [a,#], Kunji Chen [a], Zhigang Zou [b]

[a] *National Laboratory of Solid State Microstructures/School of Electronics Science and Engineering/Collaborative Innovation Center of Advanced Microstructures, Nanjing University, Nanjing 210093, Jiangsu, China*

[b] *College of Engineering and Applied Sciences, Nanjing University, Nanjing 210093, Jiangsu, China*

ARTICLE INFO

Article history:
Received 12 December 2021
Accepted 8 February 2022
Available online 20 May 2022

Keywords:
Solar hydrogen production
3D radial tandem junction
Amorphous silicon photocathode
Very thin absorber
High onset potential

ABSTRACT

Combining a progressive tandem junction design with a unique Si nanowire (SiNW) framework paves the way for the development of high-onset-potential photocathodes and enhancement of solar hydrogen production. Herein, a radial tandem junction (RTJ) thin film water-splitting photocathode has been demonstrated experimentally for the first time. The photocathode is directly fabricated on vapor-liquid-solid-grown SiNWs and consists of two radially stacked *p-i-n* junctions, featuring hydrogenated amorphous silicon (a-Si:H) as the outer absorber layer, which absorbs short wavelengths, and hydrogenated amorphous silicon germanium (a-SiGe:H) as the inner layer, which absorbs long wavelengths. The randomly distributed SiNW framework enables highly efficient light-trapping, which facilitates the use of very thin absorber layers of a-Si:H (~50 nm) and a-SiGe:H (~40 nm). In a neutral electrolyte (pH = 7), the three-dimensional (3D) RTJ photocathode delivers a high photocurrent onset of 1.15 V *vs.* the reversible hydrogen electrode (RHE), accompanied by a photocurrent of 2.98 mA/cm^2 at 0 V *vs.* RHE, and an overall applied-bias photon-to-current efficiency of 1.72%. These results emphasize the promising role of 3D radial tandem technology in developing a new generation of durable, low-cost, high-onset-potential photocathodes capable of large-scale implementation.

© 2022, Dalian Institute of Chemical Physics, Chinese Academy of Sciences.
Published by Elsevier B.V. All rights reserved.

1. Introduction

To mitigate the increasing threat of climate change and assure long-term energy security, collecting solar energy and converting it into energy-dense hydrogen is an attractive strategy [1–11]. Photoelectrochemical (PEC) water splitting is one of the most efficient routes to the production of clean and sustainable solar fuels [12–22]. To enable practical and competitive PEC hydrogen production, it is important to choose a suitable photo-absorber material, which should be made from low-cost earth-abundant elements via an economic, scalable processing technique. Therefore, silicon-based semiconductors are the most promising candidate materials among the available photo-absorber materials, owing to their abundance and the existence of mature techniques for manipulating their properties [23–33].

* Corresponding author. E-mail: zsli@nju.edu.cn
# Corresponding author. E-mail: yulinwei@nju.edu.cn

This work was supported by the National Natural Science Foundation of China (11874198, 61921005, U1663228, 51902153, 51972165), National Key Research and Development Program of China (2018YFA0209303), A Project Funded by the Priority Academic Program Development of Jiangsu Higher Education Institutions, and the Program B for Outstanding PhD candidate of Nanjing University.
DOI: 10.1016/S1872-2067(21)64046-9 | http://www.sciencedirect.com/journal/chinese-journal-of-catalysis | Chin. J. Catal., Vol. 43, No. 7, July 2022

In recent years, photocathodes for water splitting based on single-crystal silicon (c-Si) have attracted considerable attention [1,13,28,32,34–36]. However, using these c-Si based photocathodes to achieve a high onset potential (V_{onset}), for example > 0.8 V *vs.* RHE, so as to match well with that of $BiVO_4$, Fe_2O_3, and Ta_3N_5 top/front photoanodes, remains a challenge, owing to its narrow bandgap of 1.1 eV [23,37,38]. In comparison, hydrogenated amorphous silicon (a-Si:H), which has a wider band gap (~1.8 eV), can be used as a water-splitting photocathode with a high V_{onset} [27,35,38–41]. An a-Si:H-based single-junction photocathode has been reported to yield a high V_{onset} of 0.93 V *vs.* RHE [23]. However, the improvement in V_{onset} resulting from the use of a-Si:H-based photocathodes is at the expense of reduced solar spectrum utilization. To maximize solar spectrum utilization and simultaneously achieve a substantially high V_{onset} on an a-Si:H-based-thin-film photocathode, it would be beneficial to create a *p-i-n-p-i-n* tandem structure containing two photoabsorber materials [14,37,42]. In such a tandem structure, a wide-bandgap a-Si:H-based *p-i-n* junction would be employed as the top cell, and a narrow-bandgap material, such as hydrogenated amorphous silicon germanium (a-SiGe:H, with a band gap of 1.1–1.8 eV; varied by the Ge content), is used as the light-absorbing layer in the bottom cell; such a tandem-junction configuration can harvest a broader light absorption spectrum and deliver a high photo-voltage [35,39,43,44].

Because the disorder and defective matrix in a-Si:H thin films result in low carrier diffusion lengths, conventional two-dimensional (2D) planar tandem photovoltaic devices involve a trade-off between efficient carrier collection (short carrier separation distance) and sufficient light absorption (large optical absorption thickness) [45,46]. This dilemma, encountered in conventional planar junction structures, can be addressed by constructing three-dimensional (3D) a-Si:H radial-junction thin-film photovoltaic devices directly on a standing Si nanowire (SiNW) framework prepared *via* the vapor-liquid-solid (VLS) process [47–53]. The 3D SiNW framework can help to decouple the light absorption path and photocarrier extraction lengths because of the powerful light trapping effect realized among these structures, allowing the use of a very thin intrinsic light absorption layer (<100 nm) without sacrifice of sufficient light harvesting. This can improve stability against light-soaking, increase material quality tolerance, and reduce the need for high-quality and costly materials [52,54–56]. Therefore, combining a VLS-grown 3D SiNW framework with tandem junction design to fabricate radial tandem junction (RTJ) units, using a-Si:H as the outer *p-i-n* junction and a-SiGe:H as the inner layer, represents a new and promising strategy for realizing highly efficient a-Si: H-based photocathodes.

In this study, we successfully fabricated a Si-based thin-film RTJ photocathode on a VLS-grown SiNW framework, which has not been previously reported in the literature. This randomly distributed 3D vertical-standing RTJ photocathode ensures stronger light absorption than that of the planar counterparts, as shown in Fig. 1(n), thereby allowing the use of very thin absorber layers (~50 nm a-Si:H and ~40 nm a-SiGe:H). Under 100 mW/cm^2 solar illumination, the RTJ photocathode coated with a 2.5 nm-thick Pt catalyst demonstrated a high V_{onset} of 1.15 V *vs.* RHE, accompanied by a photocurrent (J_{ph}) of 2.98 mA/cm^2 at 0 V *vs.* RHE, and an applied-bias photon-to-current efficiency (ABPE) of 1.72% in 0.1 mol/L potassium phosphate aqueous solution (KPi, pH = 7) used as electrolyte. These results indicate the significant potential of this new a-Si:H-based RTJ-structured photocathode to achieve a high V_{onset} and contribute to next-generation high-efficiency, low-cost, and durable solar hydrogen production devices.

2. Experimental

2.1. Device fabrication

The fabrication process of the RTJ photocathode is shown schematically in Figs. 1(a)–(d). First, a 4 nm-thick Sn layer was

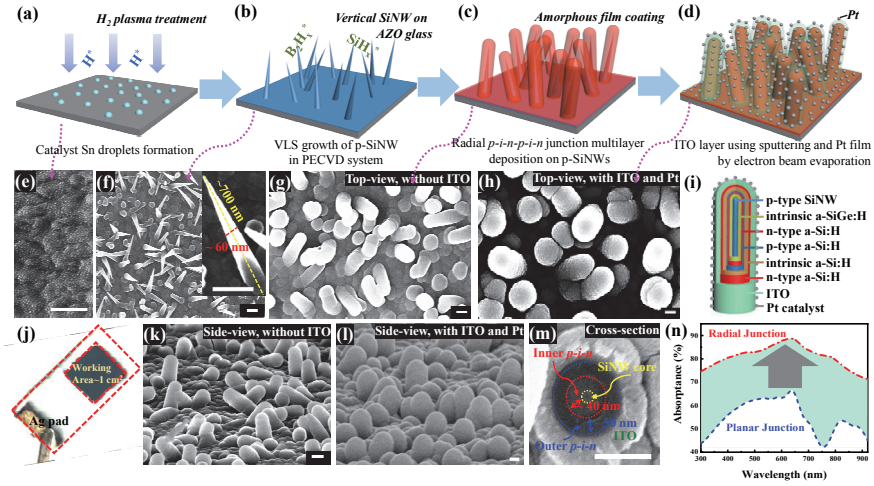


Fig. 1. (a–d) Schematic illustration of the fabrication procedures of RTJs. SEM images of H_2-plasma-treated Sn catalyst droplets (e) and VLS-grown p-type SiNWs (f). Top view of RTJ without ITO (g) and with ITO/Pt (h). Side view without ITO (k) and with ITO/Pt catalyst (l). (i) Final fabricated RTJ configuration. (j) Photograph of the RTJ photocathode. (m) Cross-section SEM image of the RTJ unit. (n) Absorption curves of radial junction and planar junction. Scale bar in (e) is 300 nm, while the others are 200 nm.

evaporated onto Al-doped zinc oxide (AZO) glass. This AZO glass substrate was then placed in a plasma-enhanced chemical vapor deposition (PECVD) system and treated with H_2 plasma (5 min, 200 °C) to form discrete Sn droplets, as shown in Fig. 1(e), with a H_2 flow rate of 20 standard cubic centimeters per minute (SCCM), an RF power density of 10 mW/cm^2, and a chamber pressure of 30 Pa. Second, the growth temperature was increased to 350 °C, and a gas mixture of H_2 (60 SCCM), silane (6 SCCM), and B_2H_6 dopant (1.8 SCCM) was introduced for 15 min to prepare p-SiNWs (RF power density: 20 mW/cm^2, chamber pressure: 100 Pa), as shown in Fig. 1(f). Subsequently, an intrinsic a-SiGe:H light-absorbing layer was prepared directly over the p-type SiNWs at 150 °C by means of a plasma of H_2 (20 SCCM), SiH_4 (6 SCCM), and GeH_4 (95% H_2-diluted; 10 SCCM), and an n-type window layer was then deposited by introducing a gas mixture of H_2 (20 SCCM), SiH_4 (6 SCCM), and PH_3 (2.3 SCCM). Next, the outer stacked *p-i-n* junction was fabricated by repeating the aforementioned preparation processes but using a p-type a-Si:H layer and an intrinsic a-Si:H layer in place of the p-SiNW and a-SiGe:H layers, respectively. Subsequently, a transparent conductive layer of tin-doped indium oxide (ITO) was deposited on the RTJ units via magnetron sputtering. Finally, platinum (Pt) catalyst layers with nominal thicknesses of 2.5 and 5 nm were deposited via electron beam evaporation. The fabricated RTJ photocathode is depicted schematically in Fig. 1(i), which shows the radially stacked multilayer structure of the p-SiNW/i-a-SiGe:H/n-a-Si:H/p-a-Si:H/i-a-Si:H/n-a-Si:H/ITO/Pt catalyst.

2.2. Device characterization

The morphology of the RTJ units was characterized using scanning electron microscopy (SEM, Zeiss Sigma) and energy dispersive spectroscopy (EDS) at probing energies E_p of 3, 5, and 11 keV. Transmission electron microscopy (TEM, TecnaiG2F20) and EDS analysis were used to characterize the nanostructure of a single RTJ unit. The photocurrent density-voltage (*J-V*) curves of the RTJ solar cells were characterized under AM 1.5 G illumination conditions (Newport, Oriel Sol-1A). The PEC characteristics of the RTJ photocathode were measured in a three-electrode setup with 0.1 mol/L KPi (pH = 7) as the electrolyte, the RTJ electrode as the working electrode, Ag/AgCl as the reference electrode, and a Pt foil as the counter electrode. The light absorption spectrum was characterized using a UV-Vis-NIR spectrophotometer (UV-3600 Plus; Shimadzu).

3. Results and discussion

Fig. 1(j) shows a photograph of the RTJ units grown on the AZO substrate, which was directly deposited on the VLS-grown p-type SiNW framework. As shown in Fig. 1(f), the representative VLS-grown SiNWs, which were randomly distributed on the uneven surface of the AZO glass substrate, have a tapering shape with an average length of ~700 nm, an average diameter of ~60 nm when measured at the middle section, and a sharp tip of <20 nm diameter. The top- and side-view SEM images of the standing RTJ units with and without an ITO layer are shown in Fig. 1(g, h, k and l). These SEM images show that the radially stacked multilayer thin films are conformally deposited over the vertical SiNW framework, which enables the fabrication of high-quality 3D RTJ photocathodes/solar cells. To explore the radially stacked internal multilayer arrangement of the RTJ unit depicted in Fig. 1(i), a selected RTJ unit was broken to expose the cross-section, as shown in the SEM image in Fig. 1(m). The inner and outer cell regions exhibit slightly different contrast in the SEM images, which can be attributed to the existence of Ge; such a contrast difference allows us to approximately estimate the thicknesses of the outer a-Si:H absorber layer and inner a-SiGe:H layer to be ~50 and ~40 nm, with deposition times of 40 and 30 min, respectively. Compared with the absorber layers used in conventional planar structures, as summarized in Table S1, both absorber layers in the RTJ photocathode are much thinner (their sum is no more than 1/3 of that in the planar structure), which can significantly reduce the cost of fabrication.

To verify the radially stacked multilayer structure of the 3D RTJ photocathode, an EDS analysis was conducted to characterize its chemical composition. The probing point was set at the tip of the non-ITO-coated RTJ unit, as shown in Fig. 2(a),

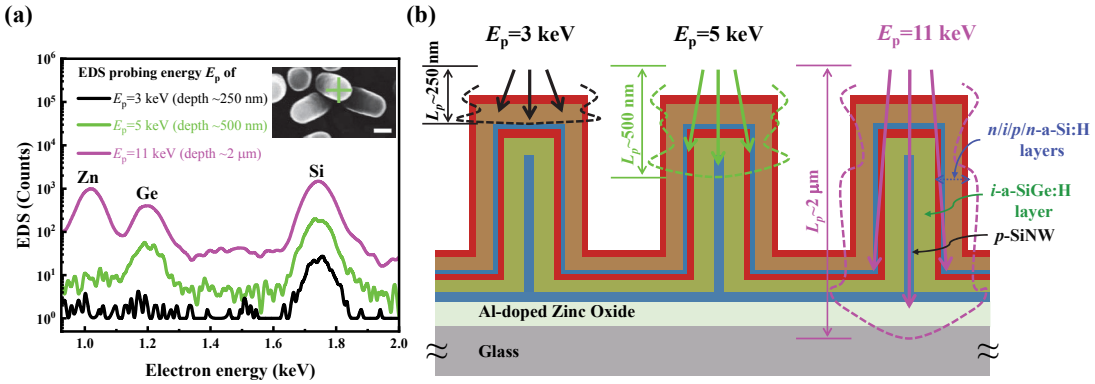


Fig. 2. (a) EDS spectra measured on the RTJ photocathode at E_p values of 3, 5, and 11 keV (without ITO layer); the detected position is indicated by a green cross in the top-right inset image, in which the scale bar represents 200 nm. (b) Different effective L_p of the EDS analysis at different probing energies.

with three different probing electron energies (E_p) of 3 keV (penetration depth ~250 nm), 5 keV (~500 nm), and 11 keV (~2 μm). The approximate effective EDS probing volumes for different values of E_p are illustrated in Fig. 2(b). Using a probing depth (L_p) of ~250 nm at E_p = 3 keV, the EDS signal (black curve in Fig. 2(a)) revealed the composition of the upper and outer segments (a-Si:H coating layers) of the RTJ unit. By increasing the E_p to 5 keV, L_p reached ~500 nm and the inner a-SiGe:H layer could be effectively probed, which was closely coated over the core p-SiNW. As the E_p was increased to 11 keV ($L_p \approx 2$ μm), the entire RTJ unit was effectively covered as well as the surface thin film and the AZO glass substrate beneath it. Under this condition (E_p = 11 keV), a strong Zn signal was observed from the AZO thin film, as shown by the pink curve in Fig. 2(a). These EDS analysis results confirm the radially stacked multilayer structure of the RTJ units, as shown in the SEM image in Fig. 1(m). In addition, TEM characterization and EDS analysis for In, Sn, Si, Ge, and Pt were performed, as shown in Fig. 3, which provides a clear insight into the radially stacked multilayer structure. The inner a-SiGe:H junction, outer a-Si:H junction, and ITO coating can be clearly observed and distinguished in the TEM image, which corresponds well with the EDS mapping images of Si and Ge. These results confirm that the present a-Si:H/a-SiGe:H RTJ photocathode is composed of a series of radially stacked multilayers that are conformally deposited on a random-directional VLS-grown SiNW framework, transforming the main work region from the conventional 2D planar to this unique 3D vertical standing arrangement.

A PEC water-splitting cell using an a-Si:H/a-SiGe:H RTJ as the photocathode is schematically depicted in Fig. 4(a). In this PEC device, the photovoltage produced by the RTJ solar cell for splitting water does not rely on the energy band positions at the liquid/solid interface. The band diagram of the RTJ photocathode is illustrated in Fig. 4(b). Under illumination, photogenerated carriers are produced in both the outer (short-wavelength-absorbing) and inner (long-wavelength-absorbing) layers and are then separated by the internal electric fields created by the corresponding *p-i-n* junctions. The photogenerated electrons are conducted across the ITO layer to Pt, which functions as a hydrogen-evolution reaction (HER) catalyst. The photogenerated holes are collected by the AZO layer and transported to the counter electrode. To afford a deeper understanding of the light absorption/distribution patterns in the core-shell RTJ photocathode, finite-element simulations were performed using the COMSOL analysis toolkit. Fig. S3 shows *n-k* curves of the a-Si:H/a-SiGe:H thin films and the built RTJ unit under periodic boundary conditions (providing more details on the COMSOL simulation). The simulated cross- and normal-section light absorption/distribution patterns for different incident wavelengths are shown in Fig. 4(c). The short-wavelength incident light is harvested mainly by the outer a-Si:H light-absorbing layer, and the longer-wavelength light (λ > 600 nm) was mainly harvested by the inner a-SiGe:H layer.

To evaluate the performance of the a-Si:H/a-SiGe:H RTJ photocathode (with a working area of approximately 1 cm^2), the PEC properties were measured in a 0.1 mol/L KPi electrolyte (pH = 7) under standard AM 1.5 G illumination (100 mW/cm^2), as shown in Fig. 5(a). The *J-V* curves of the RTJ photocathodes under illumination and in the dark are shown in Fig. 5(b), and the ABPE curves are shown in Fig. 5(c). The ABPE values were calculated from the photocurrent–potential curves according to the formula: ABPE (photocathode, %) = (J_{ph} × V_b)/P_{total} × 100%, where J_{ph} is the photocurrent acquired under an external bias (V_b), and P_{total} is the power density of the incident light (100 mW/cm^2). The thickness of the Pt catalyst plays an important role in determining the PEC performance of the RTJ photocathode because a thicker Pt catalyst is generally preferred to ensure fast surface reaction kinetics, whereas a thinner catalyst is favorable for reducing parasitic light absorption. As the thickness of the Pt catalyst was increased, V_{onset} and ABPE first increased and then decreased, reaching their corresponding maximum values when the Pt catalyst was 2.5 nm thick. The corresponding PEC parameters of the RTJ photocathodes with different Pt catalyst thicknesses are presented in Fig. 5(d), and the light-chopping *J-V* curves of the RTJ photocathodes with 2.5 and 5 nm-thick Pt catalysts are shown in Figs.

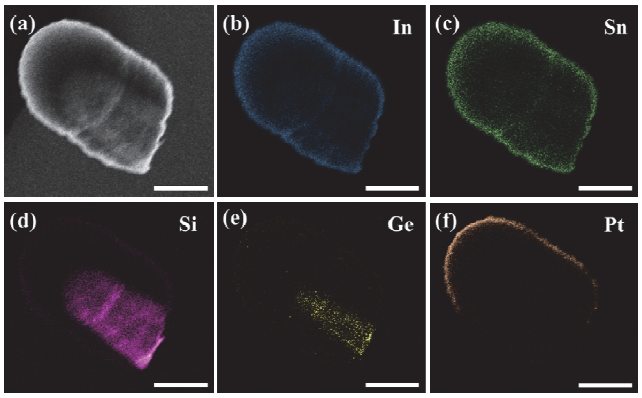


Fig. 3. TEM image (a) and EDS elemental mapping images (b–f) (In, blue; Sn, green; Si, pink; Ge, golden; Pt, orange). All scale bars are 200 nm.

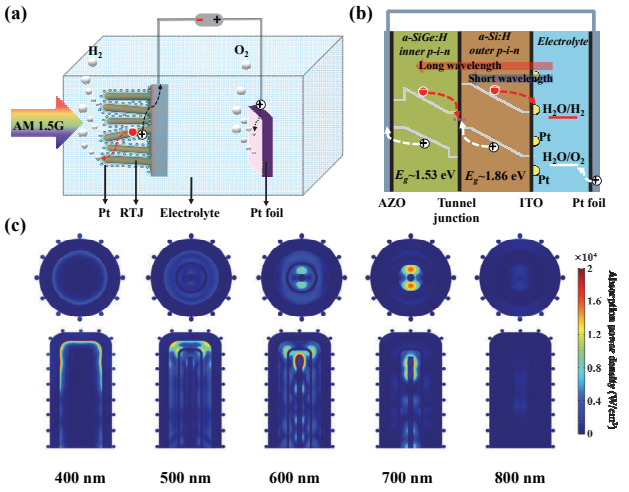


Fig. 4. (a) Schematic drawing of the PEC device under operation with the RTJ photocathode, with hydrogen evolution occurring at the RTJ photocathode. (b) Corresponding band diagram of the RTJ photocathode. (c) COMSOL-simulated light absorption patterns of cross-sections (at 1/4 height) and vertical sections (in the y-plane) of the RTJs at different incident wavelengths.

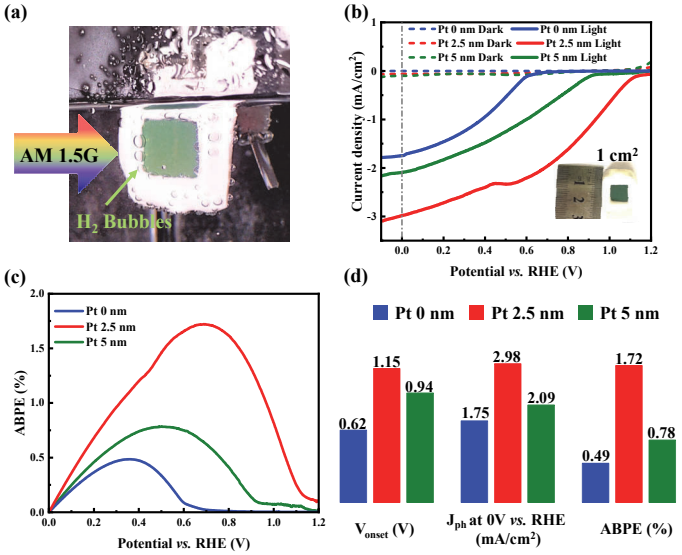


Fig. 5. (a) Photograph of the RTJ photocathode working in 0.1 mol/L KPi electrolyte (pH 7). *J-V* (b) and ABPE (c) curves for the RTJ photocathodes with different thicknesses of the Pt catalyst. (d) Extracted values of V_{onset}, J_{ph} (at 0 V *vs.* RHE), and ABPE with different nominal thicknesses of the Pt catalyst.

S4(a) and S4(b). The smaller transient currents of the 2.5 nm Pt-coated RTJ photocathode directly reflect its better charge extraction compared with that of the 5 nm Pt-coated photocathode. After the fine-tuning of the Pt catalyst, the RTJ photocathode can attain a high V_{onset} of 1.15 V *vs.* RHE, accompanied by a J_{ph} of 2.98 mA/cm² at 0 V *vs.* RHE and an ABPE of 1.72%, significantly surpassing the performance of radial single-junction units prepared in the same batch (V_{onset} 0.68 V; J_{ph} 3.13 mA/cm² at 0 V *vs.* RHE; ABPE 0.75%), as observed in Fig. S4(c). For the a-Si:H/a-SiGe:H planar tandem-junction (PTJ) thin-film photocathodes (with the 2.5 nm Pt catalyst; pink dotted line in Fig. S4(c)), a slightly lower V_{onset} of 1.10 V was obtained, which can be attributed to the thicker Pt catalyst or larger Pt nanoparticles on the smooth surface of the PTJ units, with the same nominal thickness from the same electron beam evaporation, as shown in Figs. S5(e) and S5(f). In addition, a much larger J_{ph} was achieved by the RTJ photocathodes, which emphasizes the critical role played by the powerful light trapping in the 3D RTJ matrix.

To understand the key factors that influence the PEC performance of the RTJ photocathodes, the photovoltaic characteristics of the RTJ solar cells were measured. Figs. 6(a) and

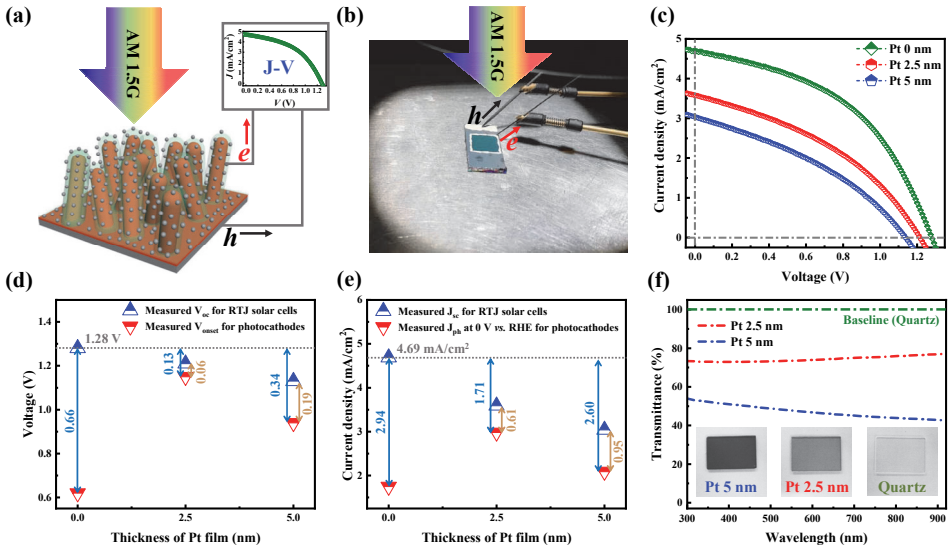


Fig. 6. Schematic diagram (a) and a photograph (b) of the test condition. (c) *J-V* curves of the RTJ solar cells with different thicknesses of the Pt catalyst. Values of V_{oc} and V_{onset} (d) and J_{sc} and J_{ph} (at 0 V *vs.* RHE) (e) of the RTJ solar cells and photocathodes for different thicknesses of the Pt catalyst. (f) Transmission spectra of the catalysts with different Pt thicknesses, with photographs of the Pt catalysts deposited on quartz. To remove the effect of the quartz, a baseline was obtained by placing quartz at the measuring location.

6(b) show a schematic diagram and a photograph of the test conditions for the RTJ solar cells (working area 1 cm^2) under standard AM 1.5 G illumination. The measured *J-V* curves for RTJ solar cells with various Pt catalyst thicknesses are shown in Fig. 6(c). The RTJ solar cells without the deposited Pt catalyst can achieve a high open-circuit voltage (V_{oc}) of 1.28 V, a short-circuit current (J_{sc}) of 4.69 mA/cm^2, a filling factor (FF) of 46.01%, and an overall power conversion efficiency (η) of 2.76%. The key performance parameters, such as V_{oc}, J_{sc}, and η, for Pt-coated RTJ solar cells were extracted and are presented in Figs. 6(d) and (e) (with corresponding V_{onset} and J_{ph} values at 0 V *vs.* RHE when functioning as water-splitting photocathodes) and Fig. S5(a). The V_{oc}, J_{sc}, and η of Pt-coated RTJ solar cells always decrease with an increase in the Pt catalyst thickness, while the values of V_{onset} and J_{ph} at 0 V *vs.* RHE demonstrate diverse trends that first increase and then decrease, with their peak values obtained at a Pt catalyst thickness of 2.5 nm. The monotonous decreasing trend of V_{oc} and J_{sc} for RTJ solar cells with the increasing Pt catalyst thickness can be attributed to the diminishing transparency of the Pt catalyst, as shown in Fig. 6(f) and illustrated by photographs of the Pt catalyst deposited on quartz. Under these conditions, the incident light that should be absorbed by the absorber layers is significantly reduced. However, eliminating the Pt catalyst from the RTJ photocathode only results in a V_{onset} of 0.62 V and a J_{ph} of 1.75 mA/cm^2 at 0 V *vs.* RHE, constituting a voltage loss of 0.66 V and a photocurrent loss of 2.94 mA/cm^2 when compared with its solar cell counterpart. Therefore, when used as water-splitting photocathodes, Pt catalysts are important for RTJ electrodes because of their surface catalytic capability. When the thickness of the Pt catalyst is optimized at 2.5 nm, providing a good balance between catalytic activity and light absorption, a minimized voltage loss of 0.06 V and photocurrent loss of 0.61 mA/cm^2 can be achieved with the RTJ photocathode.

To further elucidate the performance trends of various RTJ photocathodes, electrochemical impedance spectroscopy (EIS) measurements were conducted at 1 and 0.7 V *vs.* RHE in 0.1 mol/L KPi electrolyte (pH = 7) and under light irradiation, as shown in Figs. 7(a) and 7(b), and the fitting curves are presented in Figs. S6(b) and S6(c). When a potential of 1 V *vs.* RHE was applied, as shown in Fig. S6(b), the semi-circle representing the charge transfer resistance (R_{ct}) of the RTJ photocathode with a 2.5 nm-thick Pt catalyst coating was the lowest, with a value of ~160 Ω, which was consistent with its V_{onset} of 1.15 V, compared with 0.62 and 0.94 V *vs.* RHE for the other two photocathodes. When the applied external potential was changed from 1 to 0.7 V *vs.* RHE, as shown in Fig. S6(c), the R_{ct} of the RTJ photocathode coated with 5 nm thickness of the Pt catalyst decreased abruptly (from ~7340 to ~70 Ω). The evolution of R_{ct} with the Pt catalyst thickness is shown in Fig. S6(d). These results clearly suggest better charge extraction in the 2.5 nm-Pt-coated RTJ photocathode. The operational stability of this RTJ photocathode was evaluated over a 240 min chronoamperometry test because under this potential, it becomes active toward H_2 evolution. The J_{ph} measured at 0 V *vs.* RHE in 0.1 mol/L KPi electrolyte (pH = 7) was recorded, as shown in Fig. 7(c), and exhibited a ~10% decay over the measurement period. The decay can be attributed to the instability of the ITO coating, part of which is reduced to metallic indium and tin, resulting in poor conduction and a strong self-shade effect, as

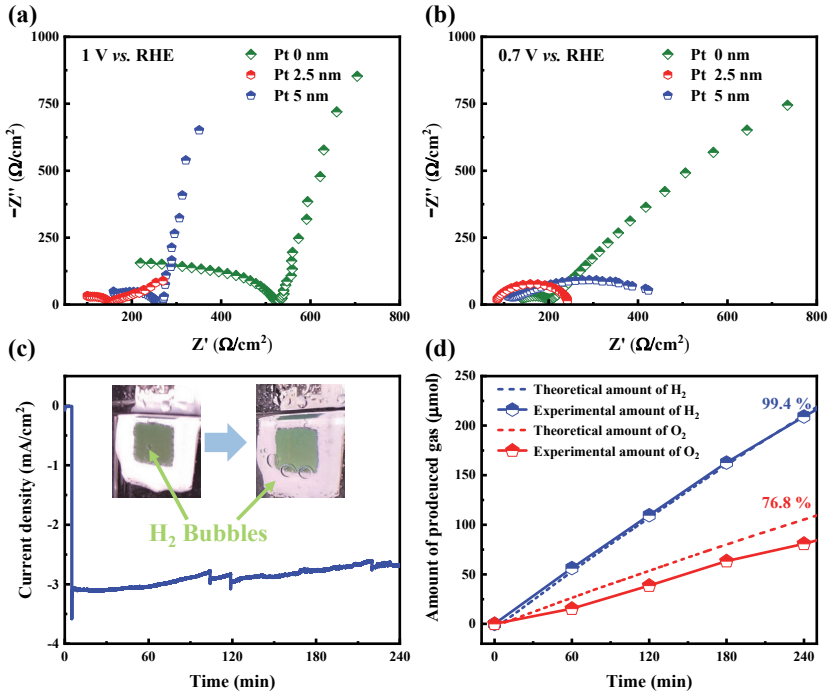


Fig. 7. EIS Nyquist plots of RTJ photocathodes with different thicknesses of the Pt catalyst at 1 V *vs.* RHE (a) and 0.7 V *vs.* RHE (b). (c) Chronoamperometric stability test of the RTJ photocathode with the 2.5 nm Pt catalyst at the fixed potential of 0 V *vs.* RHE. (d) Measured and calculated amounts of H_2 and O_2 generated by the RTJ photocathode with the 2.5 nm Pt catalyst at 0 V *vs.* RHE.

shown in Fig. S7. In addition, considering the relatively large contact area (1 cm^2) between the electrode and electrolyte, the as-proposed RTJ photocathode shows significant potential for long-term durable solar fuel production in future, provided that a reasonable protection layer is used or the ITO layer is replaced with other conductive layers. Finally, Faradaic efficiencies of H_2 and O_2 production were calculated to be 99.4% and 76.8%, respectively, as shown in Fig. 7(d), suggesting that the contributions of side reactions to the photocurrent are negligible. The lower Faradaic efficiency of O_2 production can be ascribed to the partial dissolution of O_2 in the electrolyte, resulting in the detection of a low amount of O_2.

4. Conclusions

In summary, a unique a-Si:H/a-SiGe:H-based 3D RTJ photocathode that combines a progressive tandem-junction design with a VLS-grown SiNW framework has been successfully fabricated for the first time. Owing to the strong light trapping realized among standing SiNW frameworks, very thin absorber layers are permissible, such that, for example, an a-Si:H layer of ~50 nm thickness can be used as the outer layer and an a-SiGe:H layer of ~40 nm can be utilized as the inner layer. Under AM 1.5 G illumination and in a 0.1 mol/L KPi pH 7 electrolyte, the as-fabricated RTJ photocathode coated with the 2.5 nm-thick Pt catalyst delivered a high V_{onset} of 1.15 V *vs.* RHE, a J_{ph} of 2.98 mA/cm^2 at 0 V *vs.* RHE, and an ABPE of 1.72%. These results emphasize the promising potential of this 3D RTJ design to contribute to a new generation of highly efficient and economical Si-based solar hydrogen production devices capable of large-scale implementation.

Notes

The authors declare no competing financial interest.

Electronic supporting information

Supporting information is available in the online version of this article.

References

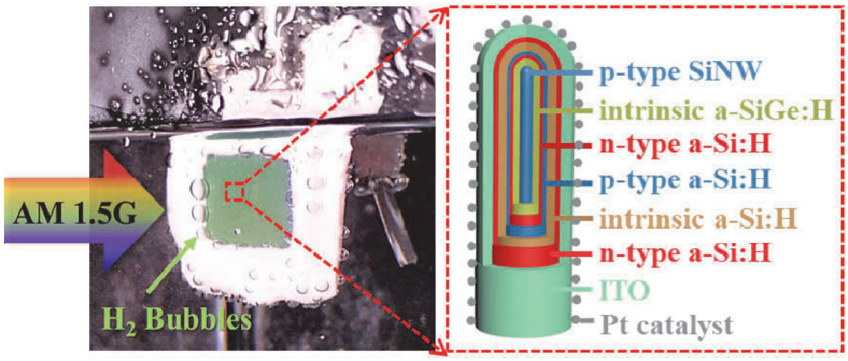
[1] R. Fan, J. Zhou, W. Xun, S. Cheng, S. Vanka, T. Cai, S. Ju, Z. Mi, M. Shen, *Nano Energy*, **2020**, 71, 104631.
[2] J. Y. Jung, J. Y. Yu, J. H. Lee, *ACS Appl. Mater. Interfaces*, **2018**, 10, 7955–7962.
[3] B. Kim, G. S. Park, Y. J. Hwang, D. H. Won, W. Kim, D. K. Lee, B. K. Min, *ACS Energy Lett.*, **2019**, 4, 2937–2944.
[4] J. Feng, H. Huang, S. Yan, W. Luo, T. Yu, Z. Li, Z. Zou, *Nano Today*, **2020**, 30, 100830.
[5] L. Ji, M. D. McDaniel, S. Wang, A. B. Posadas, X. Li, H. Huang, J. C. Lee, A. A. Demkov, A. J. Bard, J. G. Ekerdt, E. T. Yu, *Nat. Nanotechnol.*, **2015**, 10, 84–90.
[6] W. Cheng, N. Singh, W. Elliott, J. Lee, A. Rassoolkhani, X. Jin, E. W. McFarland, S. Mubeen, *Adv. Sci.*, **2018**, 5, 1700362.
[7] W.-H. Cheng, M. H. Richter, M. M. May, J. Ohlmann, D. Lackner, F. Dimroth, T. Hannappel, H. A. Atwater, H.-J. Lewerenz, *ACS Energy Lett.*, **2018**, 3, 1795–1800.
[8] Z. Li, J. Feng, S. Yan, Z. Zou, *Nano Today*, **2015**, 10, 468–486.
[9] R. R. Prabhakar, W. Septina, S. Siol, T. Moehl, R. Wick-Joliat, S. D. Tilley, *J. Mater. Chem. A*, **2017**, 5, 23139–23145.
[10] X. Wen, W. Luo, Z. Guan, W. Huang, Z. Zou, *Nano Energy*, **2017**, 41, 18–26.
[11] N. Zhang, X. Wang, J. Feng, H. Huang, Y. Guo, Z. Li, Z. Zou, *Natl. Sci.*

Graphical Abstract

Chin. J. Catal., 2022, 43: 1842–1850 doi: 10.1016/S1872-2067(21)64046-9

Ultrathin 3D radial tandem-junction photocathode with a high onset potential of 1.15 V for solar hydrogen production

Shaobo Zhang, Huiting Huang, Zhijie Zhang, Jianyong Feng, Zongguang Liu, Junzhuan Wang, Jun Xu, Zhaosheng Li *, Linwei Yu *, Kunji Chen, Zhigang Zou
Nanjing University



A radial tandem junction thin-film photocathode with a V_{onset} of 1.15 V vs. RHE has been demonstrated directly on VLS-grown SiNWs for the first time, using a-Si:H (~50 nm) as the outer absorber layer and a-SiGe:H (~40 nm) as the inner layer.

Rev., **2020**, 7, 1059–1067.
[12] J. Ran, J. Zhang, J. Yu, M. Jaroniec, S. Z. Qiao, *Chem. Soc. Rev.*, **2014**, 43, 7787–7812.
[13] R. Fan, Z. Mi, M. Shen, *Opt. Express*, **2019**, 27, A51–A80.
[14] J. Brillet, J.-H. Yum, M. Cornuz, T. Hisatomi, R. Solarska, J. Augustynski, M. Graetzel, K. Sivula, *Nat. Photonics*, **2012**, 6, 824–828.
[15] W. Yang, T. Moehl, E. Service, S. D. Tilley, *Adv. Energy Mater.*, **2021**, 11, 2003569.
[16] S. Chu, P. Ou, P. Ghamari, S. Vanka, B. Zhou, I. Shih, J. Song, Z. Mi, *J. Am. Chem. Soc.*, **2018**, 140, 7869–7877.
[17] J. Gu, Y. Yan, J. L. Young, K. X. Steirer, N. R. Neale, J. A. Turner, *Nat. Mater.*, **2016**, 15, 456–460.
[18] C. G. Morales-Guio, S. D. Tilley, H. Vrubel, M. Gratzel, X. Hu, *Nat. Commun.*, **2014**, 5, 3059.
[19] A. Paracchino, N. Mathews, T. Hisatomi, M. Stefik, S. D. Tilley, M. Grätzel, *Energy Environ. Sci.*, **2012**, 5, 8673–8681.
[20] Z. Xu, Z. Guan, J. Yang, Q. Li, *ACS Appl. Energy Mater.*, **2019**, 2, 2779–2785.
[21] J. Luo, L. Steier, M. K. Son, M. Schreier, M. T. Mayer, M. Gratzel, *Nano Lett.*, **2016**, 16, 1848–1857.
[22] L. Pan, J. H. Kim, M. T. Mayer, M.-K. Son, A. Ummadisingu, J. S. Lee, A. Hagfeldt, J. Luo, M. Grätzel, *Nat. Catal.*, **2018**, 1, 412–420.
[23] Y. Lin, C. Battaglia, M. Boccard, M. Hettick, Z. Yu, C. Ballif, J. W. Ager, A. Javey, *Nano Lett.*, **2013**, 13, 5615–5618.
[24] S. M. Thalluri, J. Borme, K. Yu, J. Xu, I. Amorim, J. Gaspar, L. Qiao, P. Ferreira, P. Alpuim, L. Liu, *Nano Res.*, **2018**, 11, 4823–4835.
[25] M. J. Choi, J.-Y. Jung, M.-J. Park, J.-W. Song, J.-H. Lee, J. H. Bang, *J. Mater. Chem. A*, **2014**, 2, 2928.
[26] R. Fan, W. Dong, L. Fang, F. Zheng, M. Shen, *J. Mater. Chem. A*, **2017**, 5, 18744–18751.
[27] C. Li, T. Wang, B. Liu, M. Chen, A. Li, G. Zhang, M. Du, H. Wang, S. F. Liu, J. Gong, *Energy Environ. Sci.*, **2019**, 12, 923–928.
[28] D.-B. Zhang, X.-J. Zhao, G. Seifert, K. Tse, J. Zhu, *Natl. Sci. Rev.*, **2019**, 6, 532–539.
[29] G. Xu, Z. Xu, Z. Shi, L. Pei, S. Yan, Z. Gu, Z. Zou, *ChemSusChem*, **2017**, 10, 2897–2903.
[30] Z. Xia, X. Zhou, J. Li, Y. Qu, *Sci. Bull.*, **2015**, 60, 1395–1402.
[31] B. Seger, S. D. Tilley, T. Pedersen, P. C. K. Vesborg, O. Hansen, M. Grätzel, I. Chorkendorff, *J. Mater. Chem. A*, **2013**, 1, 15089–15094.
[32] B. Seger, T. Pedersen, A. B. Laursen, P. C. Vesborg, O. Hansen, I. Chorkendorff, *J. Am. Chem. Soc.*, **2013**, 135, 1057–1064.
[33] G. Xie, S. U. Jan, Z. Dong, Y. Dai, R. Boddula, Y. Wei, C. Zhao, Q. Xin, J.-N. Wang, Y. Du, L. Ma, B. Guo, J. R. Gong, *Chin. J. Catal.*, **2020**, 41, 2–8.
[34] E. L. Warren, J. R. McKone, H. A. Atwater, H. B. Gray, N. S. Lewis, *Energy Environ. Sci.*, **2012**, 5, 9653.
[35] S. Y. Reece, J. A. Hamel, K. Sung, T. D. Jarvi, A. J. Esswein, J. J. H. Pijpers, D. G. Nocera, *Science*, **2011**, 334, 645–648.
[36] P. Xu, J. Feng, T. Fang, X. Zhao, Z. Li, Z. Zou, *RSC Adv.*, **2016**, 6, 9905–9910.
[37] W. Calvet, E. Murugasen, J. Klett, B. Kaiser, W. Jaegermann, F. Finger, S. Hoch, M. Blug, J. Busse, *Phys. Chem. Chem. Phys.*, **2014**, 16, 12043–12050.
[38] J. Ziegler, B. Kaiser, W. Jaegermann, F. Urbain, J. P. Becker, V. Smirnov, F. Finger, *ChemPhysChem*, **2014**, 15, 4026–4031.
[39] B. Liu, Z. Jin, L. Bai, J. Liang, Q. Zhang, C. Liu, Y. Zhao, X. Zhang, *J. Mater. Chem. A*, **2015**, 3, 15583–15590.
[40] C. G. Morales-Guio, K. Thorwarth, B. Niesen, L. Liardet, J. Patscheider, C. Ballif, X. Hu, *J. Am. Chem. Soc.*, **2015**, 137, 7035–7038.
[41] D. Zhang, Y. Cao, S. K. Karuturi, M. Du, M. Liu, C. Xue, R. Chen, P. Wang, J. Zhang, J. Shi, S. F. Liu, *ACS Appl. Energy Mater.*, **2020**, 3, 4629–4637.
[42] J. Fang, Q. Ren, F. Wang, C. Wei, B. Yan, Y. Zhao, X. Zhang, *Sol. Energy Mater. Sol. C.*, **2018**, 185, 307–311.
[43] E. Maruyama, S. Okamoto, A. Terakawa, W. Shinohara, M. Tanaka, S. Kiyama, *Sol. Energy Mater. Sol. C.*, **2002**, 74, 339–349.
[44] S. Okamoto, E. Maruyama, A. Terakawa, W. Shinohara, S. Nakano, Y. Hishikawa, K. Wakisaka, S. Kiyama, *Sol. Energy Mater. Sol. C.*, **2001**, 66, 85–94.
[45] J. Kudrna, F. Trojánek, P. Malý, I. Pelant, *Appl. Phys. Lett.*, **2001**, 79, 626–628.
[46] L. Yang, A. Catalano, R. R. Arya, I. Balberg, *Appl. Phys. Lett.*, **1990**, 57, 908–910.
[47] S. Qian, S. Misra, J. Lu, Z. Yu, L. Yu, J. Xu, J. Wang, L. Xu, Y. Shi, K. Chen, P. R. I. Cabarrocas, *Appl. Phys. Lett.*, **2015**, 107, 043902.
[48] Z. Yu, J. Lu, S. Qian, S. Misra, L. Yu, J. Xu, L. Xu, J. Wang, Y. Shi, K. Chen, P. R. I. Cabarrocas, *Appl. Phys. Lett.*, **2015**, 107, 163105.
[49] S. Misra, L. Yu, M. Foldyna, P. R. I. Cabarrocas, *Sol. Energy Mater. Sol. C.*, **2013**, 118, 90–95.
[50] J. Cho, B. O'Donnell, L. Yu, K.-H. Kim, I. Ngo, P. R. I. Cabarrocas, *Prog. Photovolt: Res. Appl.*, **2013**, 21, 77–81.
[51] S. Zhang, T. Zhang, L. Cao, Z. Liu, J. Wang, J. Xu, K. Chen, L. Yu, *Opt. Express*, **2019**, 27, 37248–37256.
[52] S. Misra, L. Yu, W. Chen, M. Foldyna, P. R. i. Cabarrocas, *J. Phys. D-Appl. Phys.*, **2014**, 47, 393001.
[53] L. Yu, F. Fortuna, B. O'Donnell, T. Jeon, M. Foldyna, G. Picardi, P. R. i. Cabarrocas, *Nano Lett.*, **2012**, 12, 4153–4158.
[54] N. S. Lewis, *Science*, **2007**, 315, 798–801.
[55] B. Tian, X. Zheng, T. J. Kempa, Y. Fang, N. Yu, G. Yu, J. Huang, C. M. Lieber, *Nature*, **2007**, 449, 885–889.
[56] T. Zhang, J. Wang, L. Yu, J. Xu, P. R. i. Cabarrocas, *Nanotechnology*, **2019**, 30, 302001.

超薄三维径向结叠层高开启电位(1.15V)光阴极用于太阳能制氢

张少波[a], 黄辉庭[b], 张之杰[a], 冯建勇[b], 刘宗光[a], 王军转[a], 徐　骏[a], 李朝升[b,*], 余林蔚[a,#], 陈坤基[a], 邹志刚[b]

[a]南京大学固体微结构物理国家重点实验室, 电子科学与工程学院, 人工微结构科学与技术协同创新中心, 江苏南京210093
[b]南京大学现代工程与应用科学学院, 江苏南京210093

摘要: a-Si:H薄膜中存在的无序结构和缺陷会大幅减小载流子扩散长度. 因此, 传统的二维平面叠层光伏器件需要在有效的载流子收集(较短的载流子分离距离)和足够的光吸收(较厚的光吸收层厚度)之间平衡. 三维a-Si:H径向结薄膜光伏器件可以很好地解决传统平面结中这一难题, 它是直接在气-液-固法生长的竖直站立的硅纳米线框架上构建. 三维硅米线框架具有很强的光捕获能力, 允许使用十分薄的光吸收层(<100 nm), 有助于解除光学吸收长度与电学载流子收集路径之间的

耦合. 薄的吸收层有助于改善光致衰减, 提升对材料质量的容忍程度, 降低对高品质、成本贵的材料的需求.

本文提出了将先进的叠层设计与独特的三维硅纳米线框架相结合的新策略, 设计了具有高开启电位的光电阴极, 以推动太阳能制氢的应用进程. 提出了径向结叠层薄膜光电阴极, 其直接在气-液-固法生长的硅纳米线上构筑, 由两个径向堆叠的*p-i-n*结组成. 外层*p-i-n*结的吸收层为非晶硅, 用于吸收短波长的光; 内层*p-i-n*结的吸收层则为非晶硅锗合金, 用于吸收长波长的光. 随机分布的硅纳米线框架具有优异的陷光效应, 可允许使用非常薄的非晶硅(~50 nm)和非晶硅锗(~40 nm)吸收层. 在100 mW/cm^{2}的太阳光照射下, 该径向结叠层光阴极在覆盖2.5 nm厚的Pt催化剂后, 在0.1 mol/L磷酸钾水溶液(KPi, pH=7)电解液中具有1.15 V *vs.* RHE的高开启电位, 零偏压下的光电流为2.98 mA/cm^2, 外加偏压下的光电转换效率为1.72%. 综上, 本文展现了三维径向结叠层技术的独特潜力, 有利于发展下一代高开启电位、高效、低成本、耐用、可大规模制备的光阴极.

关键词: 太阳能制氢; 三维径向串联结; 非晶硅基光电阴极; 超薄吸收层; 高起始电位

收稿日期: 2021-12-12. 接受日期: 2022-02-08. 上网时间: 2022-05-20.

*通讯联系人. 电子信箱: zsli@nju.edu.cn

#通讯联系人. 电子信箱: yulinwei@nju.edu.cn

基金来源: 国家自然科学基金(11874198, 61921005, U1663228, 51902153, 51972165); 国家重点研发项目(2018YFA0209303); 江苏高校优势学科建设工程资助项目; 南京大学优秀博士研究生创新能力提升计划B.

本文的电子版全文由Elsevier出版社在ScienceDirect上出版(http://www.sciencedirect.com/journal/chinese-journal-of-catalysis).